

# **The upper layer of the Malvinas/Falkland current: Structure, and transport near 46°S in January 2020**

*V. A. Krechik*<sup>1</sup>

Shirshov Institute of Oceanology RAS, Moscow, Russia

**Abstract.** Detailed velocity structure of the Malvinas/Falkland Current (M/FC) was studied based on the high-resolution shipborne ADCP direct current observations. The measurements were carried out along the transect located between  $58^{\circ}00' W$  and  $60^{\circ}22' W$ . The M/FC total transport in the upper 500 meters layer was 22.8 Sv ( $1 \text{ Sv} = 10^6 \text{ m}^3 \text{ s}^{-1}$ ). The measurements show the separation of the current flow into two jets: the wide and high-velocity Main jet whose average speed was  $0.52 \text{ m s}^{-1}$  and also the narrow Onshore jet. The Main jet transport was more than 62% of the total current transport. The average speed of the Onshore jet was  $0.36 \text{ m s}^{-1}$  and its transport was only 1.4 Sv (about 6% of total current transport). The low velocity zone which separates the two jets contains residuary 32% of the total volume transport.

# 1. Introduction

The Malvinas/Falkland Current (M/FC) is one of the most important elements of the Atlantic Meridional Overturning Circulation (AMOC). Numerical modeling estimates of the inflow of water from the Antarctic Circumpolar Current into the upper layer limb of the AMOC via the M/FC transport are as high as 50% of the total volume [*Piola et al.*, 2013]. The confluence of the M/FC cold and relatively fresh waters from the northern part of the Drake Passage and the warm salty waters of the Brazil Current leads to the formation a highly energetic Brazil/Malvinas Confluence (BMC) region near 38°S. This zone exerts strong influence on the climate of South America and the Southwest Atlantic. The Confluence region is also characterized by high eddy activity which creates conditions for significant modifications of the water masses (Antarctic Intermediate Water, Subantarctic Mode Water, Circumpolar Deep Water, and North Atlantic Deep Water) via mixing process [*Jullion et al.*, 2010].

The transition of the waters associated with the Subantarctic Front is not only the most important component of the ocean and atmospheric heat budget in this part of the World Ocean. It also generates the thermo-

haline shelf break front (SBF) [*Franco et al.*, 2008]. The SBF extends for approximately 2500 km along the Patagonia continental shelf [*Piola et al.*, 2010] and some tens of km offshore [*Romero et al.*, 2006]. This region is a zone of enhanced biological activity [*Brandini et al.*, 2000] and the place of zooplankton, fish, and mammals aggregation [*Campagna et al.*, 2007; *Thomson et al.*, 2001]. It makes this region important for fishing in the Atlantic Ocean [*Acha et al.*, 2004].

Generally, the M/FC plays an important role in heat redistribution between the ocean and the atmosphere and water mass mixing transformation. It is also a significant factor of the Southwest Atlantic biological productivity increase and has an effect on sedimentation processes in the Argentine Basin [*Weijer et al.*, 2015]. The detailed M/FC dynamic structure is important for understanding the functionality of this system and its variability. This study is focused on the M/FC velocity structure, dynamics, and transport observed in January 2020.

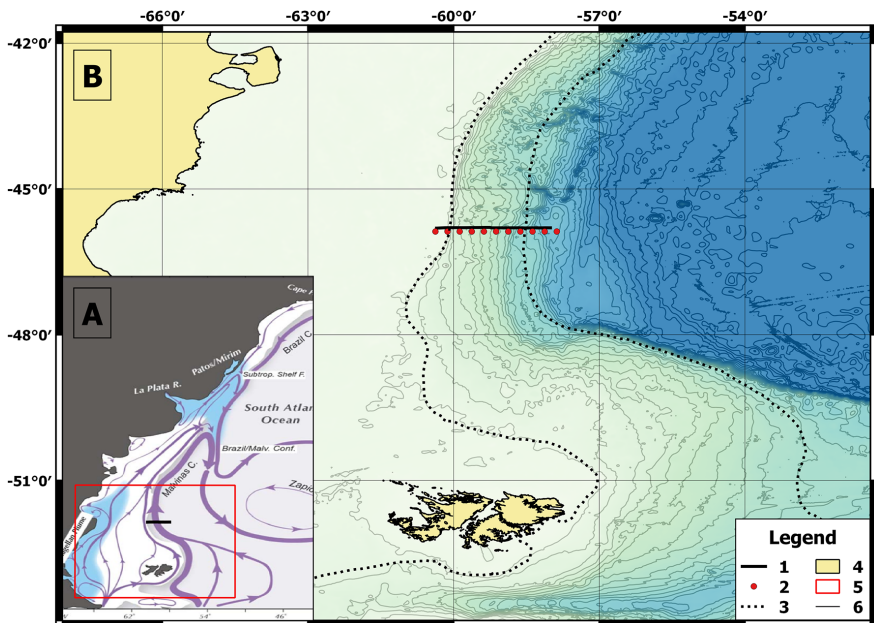


**Figure 1.** The study site. A: Circulation near the study site. The scheme was adopted from [Combes and Matano, 2014]. B: Transect location. The legend notations are: 1. Transect; 2. The grid points of the World Ocean Atlas 2013; 3. The M/FC border based on the previous studies; 4. Land; 5. Location of figure on the general map is shown in the inset; 6. Isobaths are drawn with an interval of 200 m.

## 2. Data and Methods

### 2.1. The Study Site

The region of interest is located in the western margin of the Argentine Basin near the South American continental shelf. The transect was situated at  $45^{\circ}48' S$  across the general current direction of the M/FC (Figure 1).

The M/FC volume transport has been estimated using different methods; the transport varied in a wide range [*Maamaatuaiahutapu et al.*, 1998; *Piola et al.*, 2013]. The transport estimates near the study site ( $42\text{--}46^{\circ}S$ ) using the geostrophic method vary from 3.4 Sv [*Remeslo et al.*, 2004] to 88 Sv [*Peterson*, 1992]. The numerical modeling estimates are also relatively variable: from 54 to 70 Sv [*Fetter and Matano*, 2008]. Seemingly, such difference in volume transport estimates is not only the result of using different methods for the layers of different thickness. There are the “weak” and the “strong” M/FC periods following [*Ferrari et al.*, 2017]. The “weak” M/FC is characterized by the volume transport decreasing up to 35–50% relative to the long term annual average [*Artana et al.*, 2016]. The authors of [*Paniagua et al.*, 2018] have

**Table 1.** The M/FC Volume Transports Estimates Near the Study Site Based on Direct Current Measurements

Publication	Location of the study site	Type of measurements	Estimated layer thickness, m	Transport, Sv
<i>Saunders and King, 1995</i>	near 45°S	Geostrophic calculations adjusted with direct current observations	From the surface to the bottom	50
<i>Vivier and Provost, 1999a</i>	40°–41°S	Satellite altimetry with direct current observations	From the surface to the bottom	41.5 ± 12.5
<i>Spadone and Provost, 2009</i>	40°–41°S	Satellite altimetry with direct current observations	From the surface to the bottom	35 ± 7.5
<i>Piola et al., 2013</i>	45°S	SADCP	approximately 400	20.8
<i>Morozov et al., 2016</i>	46°S	SADCP	600	20.7
<i>Morozov et al., 2016</i>	46°S	LADCP	From the surface to the bottom	30.9
<i>Artana et al., 2018</i>	40°–41°S	Current meters on moorings	From the surface to the bottom	37.1

been observing the “strong” M/FC since the beginning of January 2015 till the middle of April 2015 (104 days) and also since the middle of August till the final measurements in the end of November 2015. In the beginning of observations in December and from the middle of April 2015 till the middle of August 2015 they had been recording the “weak” M/FC. The study [*Remeslo et al.*, 2004] describes a decrease in the general current intensity in 1982–1987 and its increase in 1987–1990. The authors also show that the monthly mean volume transport had maximum values since August till October and in April. Minimal monthly mean volume transport was observed from November to February. At the same time both of the extreme values were observed in April: maximum in 1982 (12.4 Sv) and minimum in 1987 (3.4 Sv). The estimates were done for layer from the surface to 800 dbar.

There are not so many studies near our study site based on direct velocity measurements. The first observations with SADCPC at  $45^\circ$  were made in 1992 [*Saunders and King*, 1995]. The most modern study which has been done directly in the study area is [*Morozov et al.*, 2016]. The M/FC volume transport estimates near the study site based on direct current measurements are given in Table 1.

**Table 2.** Isopycnal Limits of the Water Masses *Artana et al.*, 2018

Water mass	Potential density anomaly (kg m <sup>-1</sup> ) limits	
	Upper	Lower
SASW	–	27.00
AAIW-U	27.00	27.14
AAIW-C	27.14	27.29
AAIW-L	27.29	27.35
UCDW	27.35	27.73
CDW	27.73	27.80
LCDW	27.73	27.83

The present concept of water masses near the study region is based on [*Maamaatuaiahutapu et al.*, 1994; *Piola et al.*, 2010; *Vivier and Provost*, 1999b; *Yang and He*, 2014]. The modern and thorough analysis is given in [*Artana et al.*, 2018] where seven water masses of the M/FC are distinguished based on the previous studies. These water masses and their isopycnal limits are given in (Table 2).

The study region surface layer often contains the Patagonia continental shelf waters which appear in the M/FC due to the cross-shelf water exchange. The shelf waters are usually fresher than 33.80 psu and their po-

tential density is less than  $26.5 \text{ kg m}^{-1}$  [*Piola et al.*, 2010]. *Vivier and Provost* [1999b] named these waters the Slope Waters (hereafter SW).

Generally, the M/FC thermohaline structure is relatively stable in the south near the Malvinas (Falkland) islands and becomes more complicated to the north along the current. Variations in water masses are observed near a high energy BMC zone and in the region of interaction with the Malvinas/Falkland return current.

Taking everything into account the study site as the whole M/FC is a high dynamic system with a well-defined semiannual variability. The period of variability changes from 135 [*Vivier and Provost*, 1999b; *Yang and He*, 2014] to 150 [*Fetter and Matano*, 2008] days; it is associated with the seasonal variability of the atmospheric pressure gradient between  $50^\circ$  and  $60^\circ\text{S}$  via the variations of the zonal atmospheric transport intensity over this latitudinal range. The short time variability period varies from 50 to 70 [*Vivier and Provost*, 1999b] or 90 days [*Combes and Matano*, 2014].

## 2.2. Data

The study is based on the data, which were collected during the 79-th cruise of the research vessel “*Akademik Mstislav Keldysh*”. The measurements over the transect along  $46^{\circ}\text{S}$  were made on 12 January 2020 from 16:00 to 23:20 UTC. The transect length was 186.6 km.

The data of the spatial temperature and salinity distribution at the surface were measured by the SBE 21 SeaCAT thermosalinograph with SBE3 and SBE4 sensors. The SBE Data Processing 7.20 software was used for the data processing.

The measurements of zonal and meridional velocity components were carried out using Shipborne Acoustic Doppler Current Profiler (SADCP) Teledyne RDI Ocean Surveyor 75 kHz. The data were collected using standard VmDas software. The profiler was set in the broadband mode with 90 vertical bins and 8 m blanking distance. The vessel draught was 5.6 m. The ADCP pings were averaged within 2 minutes ensembles and 8 m bins. The vessel speed varied from 7 to 10 knots. Such survey conditions and instrument settings allowed us to get high resolution data with the average horizontal cell size 520 m in the depth range from 17.6 to 460–500 m. Geographical coordinate dimensioning

was realized in WGS-84 reference system by the Trimble SPS855 GNSS-receiver. The vessel pitch and roll variations were measured by Kongsberg Seatex MRU motion sensor. The data were preprocessed and visualized during acquisition by the WinADCP software. The data with quality flag (“percent-good data” value) less than 50% were filtered out.

## 2.3. Methods

The vertical borders of water masses were derived using isopycnal limits from [*Artana et al.*, 2018] (Table 2) and also on the basis of the World Ocean Atlas 2013 (WOA 13) data. The 33.8 psu isohaline was taken as the SW lower border following [*Forbs and Garrafo*, 1988; *Piola et al.*, 2010].

The SADCPC data were de-tided using the global inverse tidal model TPXO 9.1 which is based on the satellite altimetry data [*Egbert and Erofeeva*, 2002]. This model has already shown good results near the study site [*Combes and Matano*, 2014]. Eight tidal components (semidiurnal: M2, S2, N2, K2; diurnal: K1, O1, P1, Q1) were calculated.

The volume transport was calculated as a product of the 2-min averaged cell square by the current velocity

measured in this cell. The length of each cell was calculated based on the first and last coordinates of the time averaged ensemble group. The cell length was the same for the whole depths of the averaged ensemble. The cell square was equal to the cell length multiplied by bin size (8 m). The volume transport in the  $i$ -th ensemble cell at depth  $j$  was calculated as:  $Q_{(i,j)} = v_{(i,j)}8L_i$ , where  $v_{(i,j)}$  is the current velocity measured in the cell of the ensemble number  $i$  and at depth  $j$ ,  $L_i$  is the cell length of the  $i$ -th ensemble. Only the meridional velocity component was taken into account in the calculations because of the transect orientation directly from west to east.

The borders of current structures were derived using normalization procedure. The velocity of each cell was divided by the mean of the whole data set. The cells, in which normalized velocities exceeded the mean velocity of the whole current ( $V_{\text{norm}} > 1$ ), were introduced into a high-velocity zones (jets). If normalized velocity into the cell was two times larger than the mean current velocity ( $V_{\text{norm}} > 2$ ) this cell was considered part of the jet core.

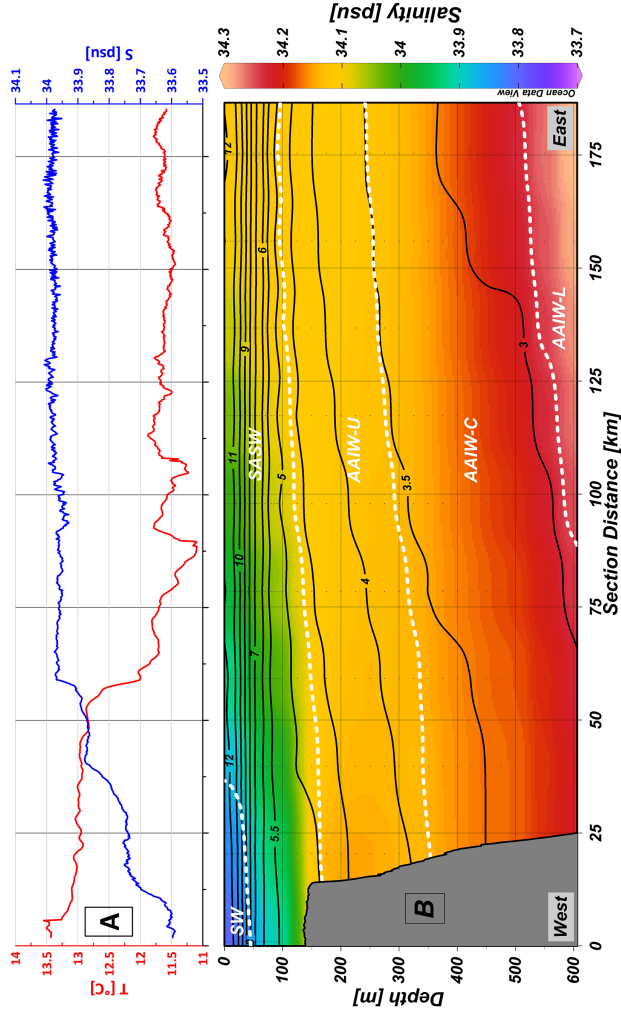


**Figure 2.** Distribution of potential temperature and salinity over the section across the Malvinas/Falkland current. A: Spatial distribution of temperature (red solid line) and salinity (blue solid line) in the surface layer along the section based on the SBE 21 thermosalinograph data. B: Potential temperature isotherms (solid black lines) over vertical salinity distribution field (color) in upper 600-m layer of the study region in January. The white dashed lines mark the borders of water masses according to its isopycnal limits. The data are based on WOA 13.

## 3. Results

### 3.1. Thermohaline Structure and Water Masses

The vertical distribution of potential temperature and salinity based on the WOA 13 data is shown in Figure 2b. The climatic data for January show the double layer vertical structure of potential temperature. The upper mixed layer (UML) is found near the surface. The UML thickness ranges from 16 to 20 m. The potential temperatures within this layer range within  $11.4^{\circ}\text{C}$ – $11.8^{\circ}\text{C}$  in the middle and eastern parts of the section. The temperature increases to  $12.6^{\circ}\text{C}$ – $12.9^{\circ}\text{C}$  in the west. The thermocline below the UML is located at a depth of about 65 m in the west and at 100–110 m in the east. The temperature monotonously decreases to the bottom below the thermocline. The isotherms are strongly inclined towards the continental slope.

Vertical salinity distribution is more complex. The shelf water and open sea water interaction leads to the formation of a large mixing zone. This zone extends for about 90 km seaward from the shelf break. At the same time the width of the shelf break front (SBF) is only about 6.5 km (Figure 2a). This zone is characterized by significant vertical and spatial gradients of

temperature and salinity. Salinity increases from 33.7 to 34.02–34.11 psu eastward. There is strong variation in salinity from 33.89 to 33.98 psu and temperature decrease in the range of 12.82°C–12.01°C inside the SBF (Figure 2a). In general, vertical salinity distribution is characterized by relatively fast increase from the surface to the bottom and halocline formation in the depth range of 40–150 m. The vertical salinity gradient in the halocline decreases eastward and then the halocline ascends and outcrops at the surface. Salinity is homogeneous below the halocline salinity up to 360–400 m and then it increases monotonously. At a depth of 600 m, salinities are 34.21–34.29 psu (Figure 2b). Five water masses are distinguished over the section in studied depth range. They are SASW, AAIW-U, AAIW-C, AAIW-L and SW (Figure 2b).

### **3.2. Dynamics and Volume Transport**

The meridional velocity component ( $V_m$ ) is positive in the entire depth range along the section excluding the eastern part. Here, negative values are observed in the surface layer (16–25 m). Seemingly, this southern current appears under the wind forcing. High velocity values are recorded in the Main jet of the current. The

Main jet western border is located approximately at a distance of 75 km from the beginning of the section (about 61 km from the shelf break). Its average width is about 68 km. The velocity in the jet increases from  $0.31 \text{ m s}^{-1}$  at the periphery to  $0.6\text{--}0.7 \text{ m s}^{-1}$  in the core. The core occupies the depths from the surface to about 400 m, and its width is 20–24 km. There are two zones where the velocity intensification is observed in the core. The maximum velocities were measured in these zones. In the subsurface zone (16–40 m depth), the velocity values are  $0.91\text{--}0.93 \text{ m s}^{-1}$ . In the zone, which is located in the depth range of 88–144 m, the maximum velocities vary from  $0.83$  to  $0.85 \text{ m s}^{-1}$  (Figure 3).

The second (Onshore) jet is located near the shelf break at a distance of 27 km from the beginning of the section; it occupies the 50–480 m depth range. Its width varies from 6 to 13 km. The Onshore jet has no explicit core. The velocity inside it varies from  $0.31$  to  $0.4 \text{ m s}^{-1}$ . There are some local zones near the Onshore jet. The velocity values in these zones are the same as in the Onshore jet stream. They could be classified as parts of the Onshore jet, which have been separated due to the interaction of the jet and the continental slope. Such zones are observed also to

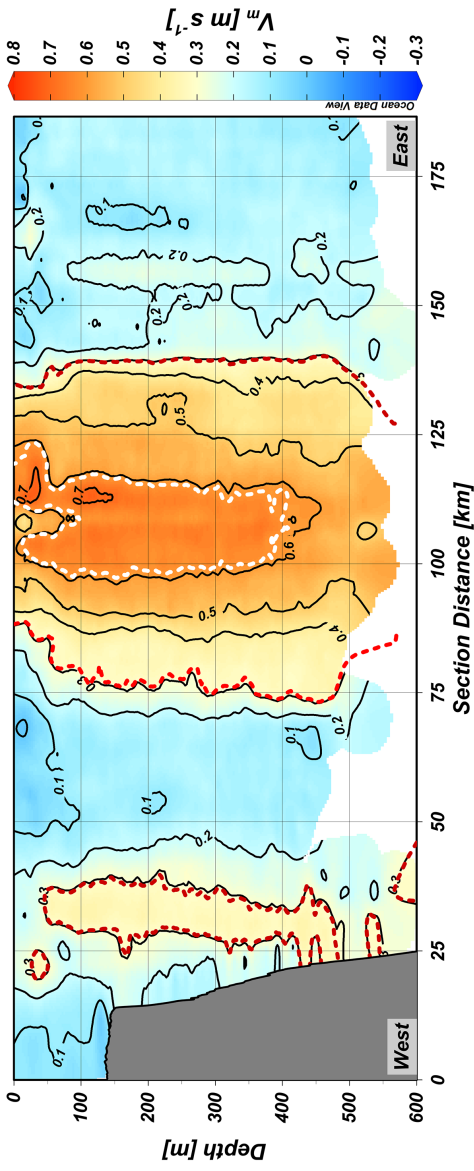


**Figure 3.** Vertical structure of the Malvinas/Falkland current meridional velocity component ( $V_m$ ) with the jets borders (red dashed line) and also the Main jet's core border (white dashed line).

the east of the Main jet in the entire depth range of the section. The descriptive statistics for  $V_m$  of the M/FC and its elements are given in Table 3.

The M/FC total volume transport is 22.82 Sv. The Main jet volume transport contains more than 62% of the total volume transport. The low dynamics areas, which separate the Main and Onshore jets, concentrate 32% of the total volume transport. The Onshore jet transport is 1.36 Sv that is ten times smaller than the Main jet transport (Table 3). The vertical distribution of transport is relatively homogeneous. The total volume transport of the upper and central AAIW subtypes is 17.52 Sv (8.36 Sv by AAIW-U and 9.15 Sv by AAIW-C). The transport of SASW, which occupies the most dynamic upper layer, is only 5.09 Sv. The SW flow in the northern direction; its transport is 0.19 Sv. There were less than 40 samples inside the AAIW-L because of its location below the 500 m depth. These samples show a transport of only 0.03 Sv.

## 4. Discussion and Conclusions

Generally, the thermohaline structure and vertical distribution of water masses are very close to that presented in [*Artana et al.*, 2018; *Paniagua et al.*, 2018].

**Table 3.** The Descriptive Statistics of Meridional Velocity Component and Also the Volume Transport of the M/FC and its Main Elements

Elements of the current	Minimum	Maximum	Average	Standard deviation	Number of counts	Area, km <sup>2</sup> (%)	Transport, Sv (%)
Main jet (without core)	0.309	0.617	0.473	0.089	4853	21.81 (29.31)	10.31 (45.17)
Main jet core	0.618	0.926	0.678	0.051	1319	5.77 (7.75)	3.92 (17.16)
Onshore jet	0.309	0.559	0.365	0.043	786	3.72 (5.00)	1.36 (5.96)
Background stream	-0.361	0.308	0.167	0.081	9474	43.13 (57.94)	7.24 (31.71)
Whole current	-0.362	0.926	0.309	0.193	16432	74.43 (100)	22.82 (100)

Spatial temperature and salinity distribution was confirmed by the SBE 21 thermosalinograph data. Salinities in the frontal zone were higher than the value of the criterion, which is usually used to separate the SW and the M/FC seawater ( $S < 33.8$  psu) [*Forbs and Garrafo*, 1988; *Piola et al.*, 2010]. The SBF extends for 90 km seaward from the shelf break as shown in [*Romero et al.*, 2006].

The meridional velocity component presents a northward flow. The highest velocity is observed inside the Main jet core, which average velocity value is  $0.68 \text{ m s}^{-1}$ . One more jet is situated at a distance of 12–14 km from the shelf break. High velocities are also observed in this jet. The average velocity value is  $0.36 \text{ m s}^{-1}$ . Such spatial structure and dynamics of the M/FC are described in [*Magalhães and da Silva*, 2017; *Painter et al.*, 2010; *Piola et al.*, 2013]. The authors of [*Piola et al.*, 2013] derive the local zones of intense velocity east of the Main jet. These zones are observed in the sections and on the surface near the main current stream from  $41^{\circ}\text{S}$  to  $47^{\circ}\text{S}$  (Fig. 6 in [*Piola et al.*, 2013]). The SADC data also show the presence of such zones east of the Main jet. They are separated or partly separated from the jet. These zones formation is related to the spatial dynamic features of the Main jet.

The Main jet transports 62.33% of the total volume transport, which is 22.82 Sv. This estimate is close to the results of direct velocity measurements in [*Pirola et al.*, 2013] (20.8 Sv up to 400 m depth) and [*Morozov et al.*, 2016] (20.7 Sv up to 600 m depth). The transports of water masses which are located up to 500 m depth are 5.09, 8.36, and 9.15 Sv for SASW, AAIW-U, and AAIW-C, respectively. Such increase of volume transport with depth shows that the barotropic component dominates in the M/FC volume transport structure. The SW transport is 0.19 Sv. This volume is about one third of the total transport of the Patagonia shelf which has been estimated as 0.65–0.78 Sv [*Palma et al.*, 2008].

**Acknowledgments.** This research was performed in the framework of the state assignment of Shirshov Institute of Oceanology No. 0128-2019-0008.

## References

- Acha, E. M., H. W. Mianzan, et al. (2004) , Marine fronts at the continental shelves of austral South America: Physical and ecological processes, *J. Mar. Syst.*, 44, p. 83–105, **Crossref**
- Artana, C., R. Ferrari, Z. Koenig, et al. (2016) , Malvinas Current

- variability from Argo floats and satellite altimetry, *J. Geophys. Res. Oceans*, 121, p. 4854–4872, **Crossref**
- Artana, C., J.-M. Lellouche, et al. (2018) , Fronts of the Malvinas Current System: Surface and subsurface expressions revealed by satellite altimetry, Argo floats, and Mercator operational model outputs, *J. Geophys. Res. Oceans*, 123, p. 5261–5285, **Crossref**
- Brandini, F. P., D. Boltovskoy, A. R. Piola, et al. (2000) , Multi-annual trends in fronts and distribution of nutrients and chlorophyll in the southwestern Atlantic (30–62 S), *Deep Sea Res., Part I*, 47, p. 1015–1033, **Crossref**
- Campagna, C., A. R. Piola, et al. (2007) , Deep divers in shallow seas: Southern elephant seals on the Patagonian shelf, *Deep Sea Res., Part I*, 54, p. 1792–1814, **Crossref**
- Combes, V., R. P. Matano (2014) , A two-way nested simulation of the oceanic circulation in the Southwestern Atlantic, *J. Geophys. Res. Oceans*, 119, p. 731–756, **Crossref**
- Egbert, G. D., S. Y. Erofeeva (2002) , Efficient inverse modeling of barotropic ocean tides, *J. Atmos. Oceanic Technol.*, 19, p. 183–204, **Crossref**
- Ferrari, R., C. Artana, M. Saraceno, et al. (2017) , Satellite altimetry and current-meter velocities in the Malvinas Current at 41°S: Comparisons and modes of variations, *J. Geophys. Res. Oceans*, 122, p. 9572–9590, **Crossref**
- Fetter, A. F. H., R. P. Matano (2008) , On the origins of the variability of the Malvinas Current in a global, eddy-permitting numerical simulation, *J. Geophys. Res.*, 113, p. C11018, **Crossref**
- Forbs, M. C., Z. Garrafo (1988) , A note on the mean seasonal

- transport on the Argentine Shelf, *J. Geophys. Res.*, 93, p. 2311–2319, [Crossref](#)
- Franco, B. C., A. R. Piola, et al. (2008) , Multiple thermal fronts near the Patagonian shelf break, *Geophys. Res. Lett.*, 35, p. L02607, [Crossref](#)
- Jullion, L., K. J. Heywood, et al. (2010) , Circulation and water mass modification in the Brazil-Malvinas Confluence, *J. Phys. Oceanogr.*, 40, p. 845–864, [Crossref](#)
- Maamaatuaiahutapu, K., V. Garçon, et al. (1994) , Spring and winter water mass composition in the Brazil-Malvinas Confluence, *J. Mar. Res.*, 52, p. 397–426, [Crossref](#)
- Maamaatuaiahutapu, K., V. Garçon, et al. (1998) , Transports of the Brazil and Malvinas Currents at their Confluence, *J. Mar. Res.*, 56, p. 417–438, [Crossref](#)
- Magalhães, J. M., J. C. B. da Silva (2017) , Internal waves along the Malvinas Current: Evidence of transcritical generation in satellite imagery, *Oceanography*, 30, no. 3, p. 110–119, [Crossref](#)
- Morozov, E. G., R. Yu. Tarakanov, T. A. Demidova, et al. (2016) , Velocity and transport of the Falkland Current at 46°S, *Russ. J. Earth. Sci.*, 16, p. ES6005, [Crossref](#)
- Palma, E. D., R. P. Matano, A. R. Piola (2008) , A numerical study of the Southwestern Atlantic Shelf circulation: Stratified ocean response to local and offshore forcing, *J. Geophys. Res.*, 113, p. C11010, [Crossref](#)
- Painter, S. C., A. J. Poulton, et al. (2010) , The COPAS-08 expedition to the Patagonian Shelf: Physical and environmental conditions during the 2008 coccolithophore bloom, *Cont. Shelf*

- Res., 30, no. 18, p. 1907–1923, [Crossref](#)
- Paniagua, G. F., M. Saraceno, A. R. Piola, et al. (2018) , Malvinas Current at 40°S–41°S: First assessment of temperature and salinity temporal variability, *J. Geophys. Res. Oceans*, 123, [Crossref](#)
- Peterson, R. G. (1992) , The boundary current in the western Argentine Basin, *Deep Sea Res., Part A*, 39, p. 623–644, [Crossref](#)
- Piola, A. R., B. C. Franco, et al. (2013) , Multiple jets in the Malvinas Current, *J. Geophys. Res. Oceans*, 118, p. 2107–2117, [Crossref](#)
- Piola, A. R., N. Martínez Avellaneda, et al. (2010) , Malvinas-slope water intrusions on the northern Patagonia continental shelf, *Ocean Sci.*, 6, p. 345–359, [Crossref](#)
- Remeslo, A. V., E. G. Morozov, et al. (2004) , Structure and variability of the Falkland Current, *Doklady Earth Sciences*, 399, p. 1156–1159.
- Romero, S. I., A. R. Piola, et al. (2006) , Chlorophyll a variability off Patagonia based on SeaWiFS data, *J. Geophys. Res.*, 111, p. C05021, [Crossref](#)
- Saunders, P. M., B. A. King (1995) , Bottom currents derived from shipborne ADCP on WOCE cruise A11 in the South Atlantic, *J. Phys. Oceanogr.*, 25, p. 329–347, [Crossref](#)
- Spadone, A., C. Provost (2009) , Variations in the Malvinas Current volume transport since October 1992, *J. Geophys. Res.*, 114, p. C02002, [Crossref](#)
- Thomson, G. A., A. A. Alder, D. Boltovskoy (2001) , Tintinnids (Ciliophora) and other net microzooplankton (> 30 μm) in southwestern Atlantic shelf break waters, *Mar. Ecol.*, 22, p.

343–355, **Crossref**

Vivier, F., C. Provost (1999a) , Volume transport of the Malvinas Current: Can the flow be monitored by TOPEX/Poseidon?, *J. Geophys. Res.*, 104, **Crossref**

Vivier, F., C. Provost (1999b) , Direct velocity measurements in the Malvinas Current, *J. Geophys. Res.*, 104, **Crossref**

Weijer, W., M. E. Maltrud, W. B. Homoky, et al. (2015) , Eddy-driven sediment transport in the Argentine Basin: Is the height of the Zapiola Rise hydrodynamically controlled?, *J. Geophys. Res. Oceans*, 120, p. 2096–2111, **Crossref**

Yang, X.-Y., Z. He (2014) , Decadal change of Antarctic Intermediate Water in the region of Brazil and Malvinas confluence, *Deep Sea Res., Part I*, 88, p. 1–7, **Crossref**

---